Korean J. Chem. Eng., **29**(3), 349-355 (2012)
DOI: 10.1007/s11814-011-0131-4

Characterizations of composite cathodes with $La_{0.6}Sr_{0.4}Co_{0.2}Fe_{0.8}O_{3-\delta}$ and $Ce_{0.9}Gd_{0.1}O_{1.95}$ for solid oxide fuel cells

Ju Hee Kim*, Young Min Park, Taejin Kim***, and Haekyoung Kim*,†**

*School of Materials Science & Engineering, Yeungnam University, Gyeongsan 712-749, Korea
**Fuel Cell Project, Research Institute of Industrial Science and Technology, Pohang 790-330, Korea
***Dae-Gyeong Leading Industry Office, Sampoong-dong, Gyeongsan 712-210, Korea
(*Received 17 March 2011 • accepted 11 May 2011*)

Abstract−Composite cathodes with $La_{0.6}Sr_{0.4}Co_{0.2}Fe_{0.8}O_{3-\delta}$ (LSCF) and $Ce_{0.9}Gd_{0.1}O_{1.95}$ (GDC) are investigated to assess for solid oxide fuel cell (SOFC) applications at relatively low operating temperatures (650-800 °C). LSCF with a high surface area of 55 m^2g^{-1} is synthesized via a complex method involving inorganic nano-dispersants. The fuel cell performances of anode-supported SOFCs are characterized as a function of compositions of GDC with a surface area of 5 m^2g^{-1}. The SOFCs consist of the following: LSCF-GDC composites as a cathode, GDC as an interlayer, yttrium stabilized zirconia (YSZ) as an electrolyte, Ni-YSZ (50 : 50 wt%) as an anode functional layer, and Ni-YSZ (50 : 50 wt%) for support. The cathodes are prepared for 6LSCF-4GDC (60 : 40 wt%), 5LSCF-5GDC (50 : 50 wt%), and 4LSCF-6GDC (40 : 60 wt%). The 5LSCF-5GDC cathode shows 1.29 Wcm^{-2}, 0.97 Wcm^{-2}, and 0.47 Wcm^{-2} at 780 °C, 730 °C, and 680 °C, respectively. The 6LSCF-4GDC shows 0.92 Wcm^{-2}, 0.71 Wcm^{-2}, and 0.54 Wcm^{-2} at 780 °C, 730 °C, and 680 °C, respectively. At 780 °C, the highest fuel cell performance is achieved by the 5LSCF-5GDC, while at 680 °C the 6LSCF-4GDC shows the highest performance. The best composition of the porous composite cathodes with LSCF (55 m^2g^{-1}) and GDC (5 m^2g^{-1}) needs to be considered with a function of temperature.

Key words: Solid Oxide Fuel Cell, Mixed Conductor, Nano Dispersant, Anode Supported Cell, Composite Cathode

INTRODUCTION

Solid oxide fuel cells (SOFCs) are believed to be the most promising future component of energy generation systems for power plants and distributed power systems. For operation at intermediate temperature (IT, 600-800 °C), lanthanum-based iron- and cobalt-containing perovskites are good candidates for SOFC cathode materials because of their high electro-catalytic activity. With a Gd-doped ceria (GDC)-based interlayer, perovskite-based compounds having the general formula of $La_{0.6}Sr_{0.4}Co_{0.2}Fe_{0.8}O_{3-\delta}$ (LSCF) have been reported to be very effective for IT-SOFC applications because of their high ionic conductivity and catalytic activity [1-7].

Electrochemical reactions occur at both the triple phase boundary (LSCF, GDC, and oxygen gas) and the surface of LSCF. However, because of the high activation enthalpy for oxygen self-diffusion (186±75 $kJmol^{-1}$) associated with LSCF [8], the ionic conductivity of an LSCF cathode drops rapidly as the temperature decreases. To enhance the ionic conductivity of the cathode electrode and prevent the coarsening of the cathode, the addition of a second phase such as GDC has been reported [9-13]. Studies have confirmed that the formation of a composite cathode can beneficially reduce the polarization resistance of a pure LSCF cathode [14-17]. This enhanced performance is related to the sintering temperature, the microstructure (such as the grain size and porosity) and the composition of the LSCF and the GDC. By addition of GDC, it is conceivable that the polarization resistance of the composite electrode decreases by extending the TPB and increasing the oxygen diffusion, which results in much lower over-potentials toward oxygen reduction. Furthermore, the pores introduced in the LSCF-GDC composite cathode in terms of the GDC surface area facilitate gas transport and accelerate electrode kinetics. The overall performance of a porous electrode is not only determined by the mixed conducting transport properties in the solid phase of the electrode, but also by the inherent catalytic property of the triple phase boundary, and by the gas transport to, or away, from the triple phase boundary [1]. The contents of GDC in the composite cathode have been studied and the 50-60 wt% of GDC in the composite cathodes shows the lower cathode polarization at 600 °C [1,13]. However, the morphology of GDC, the surface area, is uninformative and it is difficult to figure out the relationship between the morphologies and contents of GDC particles.

In this study, composite cathodes were prepared with LSCF-based nanocrystalline powders (surface area of 55 m^2g^{-1}) and GDC (surface area of 5 m^2g^{-1}). LSCF powders were prepared via a complex method involving ethylene diamine tetra-acetic acid (EDTA), citric acid, and inorganic nano-dispersants. LSCF and GDC were mixed with together in ratios of 60 : 40 wt%, 50 : 50 wt%, and 40 : 60 wt%. These pastes of LSCF and GDC were then printed and sintered onto anode-supported SOFC cells comprised of layers of Ni-YSZ (support), Ni-YSZ (functional layer), YSZ (electrolyte), and GDC (interlayer). The fuel cell performances and the impedances were characterized and analyzed in terms of the wt% of GDC and the temperature.

EXPERIMENTAL PROCEDURES

Analytical grade lanthanum nitrate, strontium nitrate, cobalt nitrate,

†To whom correspondence should be addressed.
E-mail: hkkim@ynu.ac.kr

and ferric nitrate were used as metal sources for the LSCF perovskite powders. EDTA powder and crystallized citric acid, each with a purity level higher than 99.5%, were used as the raw materials for chelation. A homogeneous metal nitrate solution was prepared by dissolving 7.79 g (0.018 mol) of lanthanum nitrate ($La(NO_3)_3 \cdot 6H_2O$), 2.53 g (0.012 mol) of strontium nitrate ($Sr(NO_3)_2$), 1.74 g of (0.006 mol) cobalt nitrate ($Co(NO_3)_2 \cdot 6H_2O$), and 9.7 g (0.024 mol) of ferric nitrate ($Fe(NO_3)_3 \cdot 9H_2O$) in 100 ml of deionized water as the previous work [18]. Next, 11.47 g (0.06 mol) of solid citric acid was added to the mixed metal nitrate solution, followed by 8.77 g (0.03 mol) of EDTA powder. The solution was then heated in a water bath at 70 °C until it became clear, at which point 3 g of HI BLACK170 carbon black was added as an inorganic nano-dispersant. To evaporate the water, the mixture was reheated until a magnetic bar immersed in the solution stopped rotating. The remaining mixture was dried overnight at 80-120 °C in a vacuum oven to remove the residual water. The dried mixture was crushed and calcined at 700 °C for 5 hours to form a perovskite phase and to remove any organic compounds and inorganic nano-dispersants.

The Ni-YSZ/YSZ/GDC anode-supported cells, which consist of Ni-YSZ of ~900 μm as a support layer/Ni-YSZ of ~20 μm as an anode functional layer (AFL)/YSZ of ~10 μm as an electrolyte, were fabricated using a tape casting and co-firing method at 1370 °C. The GDC interlayer of ~1 μm was formed on YSZ electrolyte via

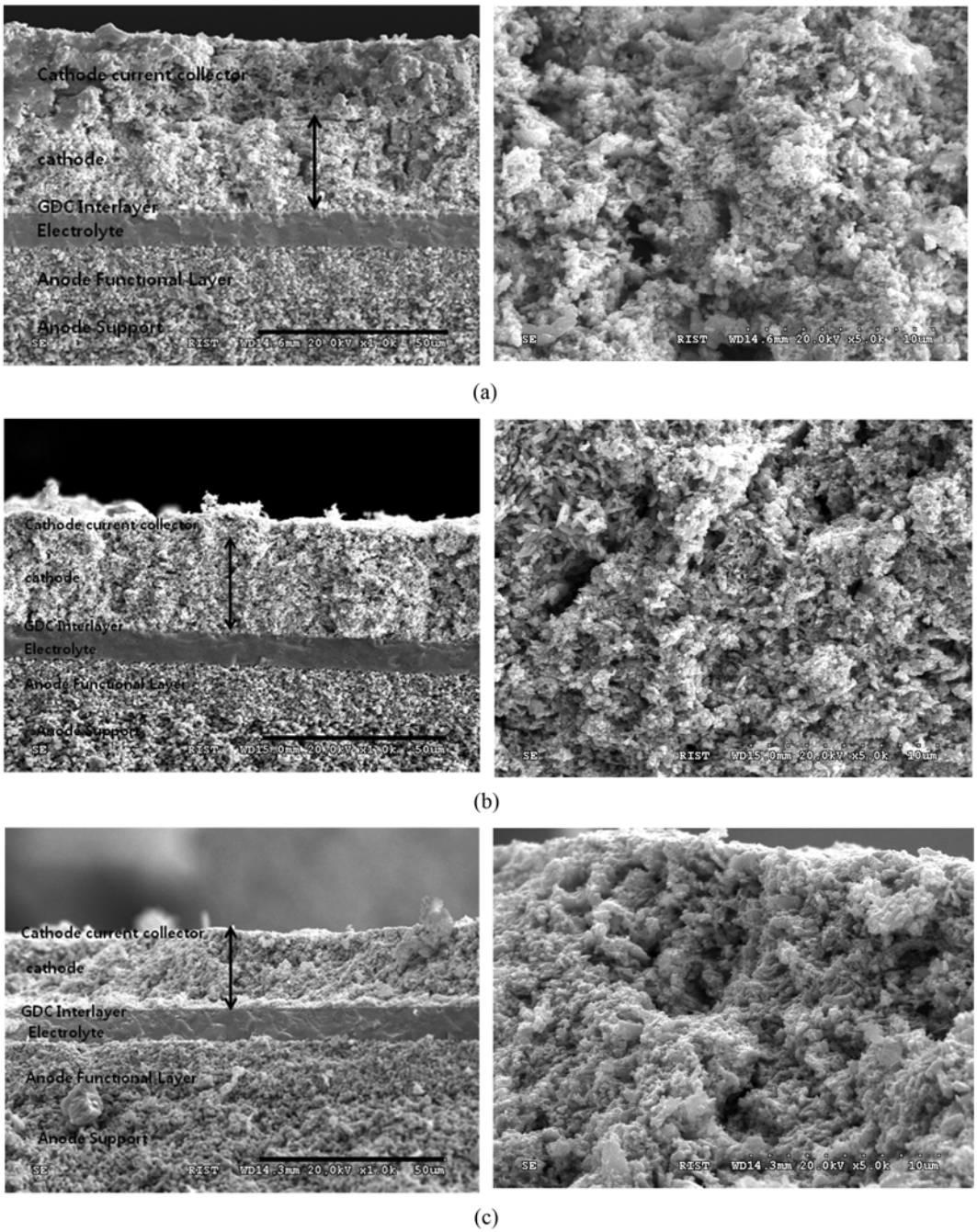

Fig. 1. Cross-sectional images of SOFC with composite cathodes of (a) 6LSCF-4GDC cathode, (b) 5LSCF-5GDC, and (c) 4LSCF-6GDC.

an aerosol deposition method. The anode-supported cells were cut into circles with diameters of 2.6 cm from a 25 cm×25 cm plate. GDC materials for composite cathodes, the surface area of 5 m^2g^{-1}, were from ANNA Kasei. LSCF and GDC was mixed in ratios of 60 : 40 wt% (6LSCF-4GDC), 50 : 50 wt% (5LSCF-5GDC), and 40 : 60 wt% (4LSCF-6GDC). A paste with ESL 449 from Electroscience was prepared and screen-printed onto the Ni-YSZ/YSZ/GDC anode-supported cell. Finally, the composite cathodes were sintered at 900 °C for 3 hrs. The active cathode area was 0.785 cm^2. The fabricated cells were assembled and sealed with Cerama bond™ 571 from AREMCO in a jig to measure current-voltage characteristic and impedances. The Pt paste and the Pt mesh were used for current collecting. Fuel cell performances were tested with 300 $ccmin^{-1}$ of 97% H_2-3% H_2O and 1,500 $ccmin^{-1}$ of air. The impedance was measured with the WEIS system from WonATech. The impedance spectra were obtained in the frequency range of 100 kHz to 0.1 Hz with applied AC voltage amplitude of 100 mV at each temperature and cell potential of OCV, 0.9 V, and 0.7 V. After electrochemical measurements, the microstructures of SOFCs were characterized with scanning electron microscopy, JSM-6480LV.

RESULTS AND DISCUSSIONS

As shown in Fig. 1, after electrochemical measurements, the cross-sectional images of the composite cathodes are characterized by using scanning electron microscopy (SEM). Good adhesion between the cathode and the GDC buffer layer is observed in all cases of the composite cathodes. The composite cathodes consist of the LSCF, with a surface area of 55 m^2g^{-1}, and the GDC, with a surface area of 5 m^2g^{-1}, and the compositions of LSCF and GDC are in ratios of 60 : 40 wt% (6LSCF-4GDC), 50 : 50 wt% (5LSCF-5GDC), and 40 : 60 (4LSCF-6GDC) wt%. The thickness of the cathodes is 20-30 μm in each composite cathode. The Pt layers for current collecting are observed in 6LSCF-4GDC and 5LSCF-5GDC cathodes. The current collector layer in 4LSCF-6GDC SOFC is not observed, which is lost in an SEM sample preparation step. The 6LSCF-4GDC cathode shows small particles and pores of 1-3 μm. With the increasing GDC content, the macro-pores of ~5 μm are more easily observed in the 5LSCF-5GDC and the 4LSCF-6GDC. The addition of GDC produces the macro-pores due to the larger particles size with increasing the GDC contents.

The current-voltage-power characteristics of SOFCs are shown in Fig. 2 and Fig. 3. The fuel cell performance increases with increasing temperature. The 6LSCF-4GDC shows the maximum power density of 0.9 Wcm^{-2}, 0.7 Wcm^{-2} and 0.52 Wcm^{-2} at 780 °C, 730 °C, and 680 °C, respectively. The 5LSCF-5GDC shows the maximum power density of 1.29 Wcm^{-2}, 0.95 Wcm^{-2}, and 0.48 Wcm^{-2} at 780 °C, 730 °C, and 680 °C, respectively. The 4LSCF-6GDC shows the maximum power density of 0.6 Wcm^{-2}, 0.48 Wcm^{-2}, and 0.3 Wcm^{-2} at 780 °C, 730 °C, and 680 °C, respectively. The fuel cell performances with composite cathodes at each temperature are shown in Fig. 3. At 780 °C, and 730 °C, the 5LSCF-5GDC shows the highest fuel cell performance of 1.29 Wcm^{-2} and 0.95 Wcm^{-2}, respectively. However, at 680 °C the 6LSCF-4GDC shows the highest maximum power density of 0.58 Wcm^{-2}. The fuel cell performance with cathode depends on the factors from the materials and process such as composition, sintering temperature, and morphology. The effects of GDC

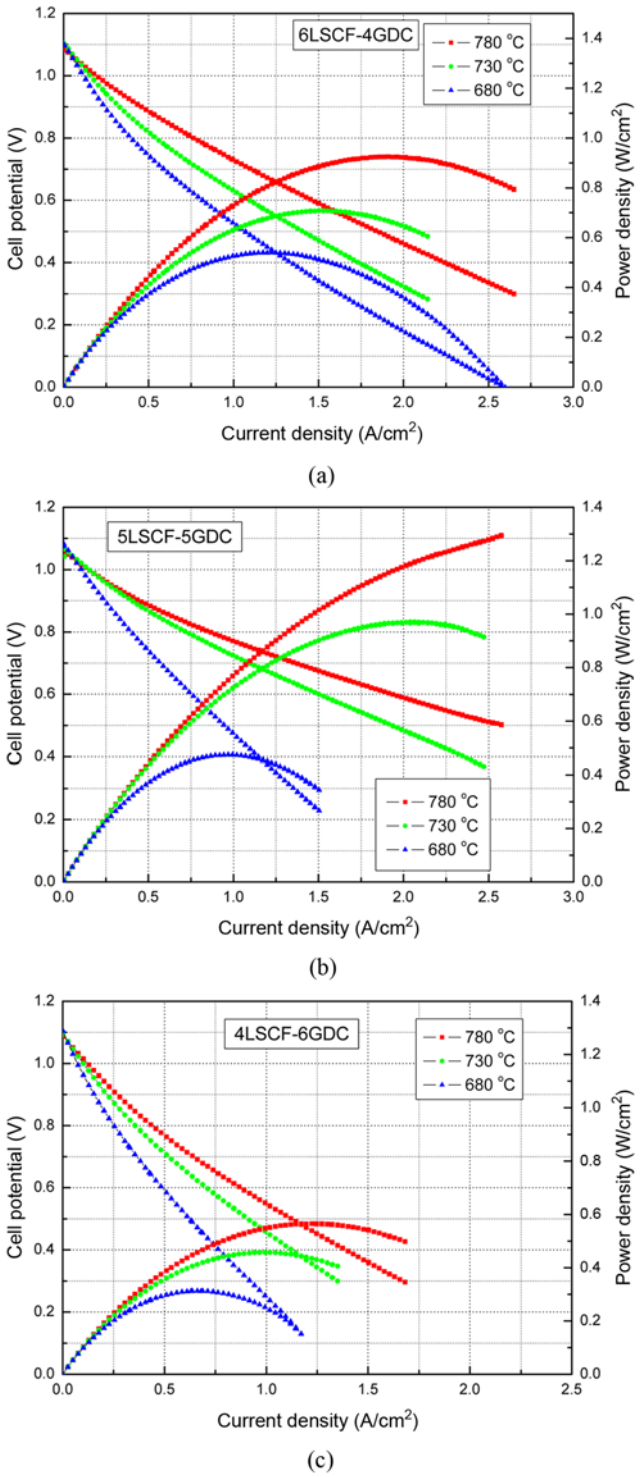

Fig. 2. Fuel cell performances of SOFCs with composite cathodes of (a) 6LSCF-4GDC cathode, (b) 5LSCF-5GDC, and (c) 4LSCF-6GDC.

depend on the morphology of the starting GDC materials. Here, the surface area of GDC and LSCF is 5 m^2g^{-1} and 55 m^2g^{-1}, respectively. The triple phase boundaries for the electrochemical reactions are a function of the morphologies of LSCF and GDC. The morphologies concerned with the pores formed with particles are also a factor for the electrochemical reactions. The composite cath-

ode of LSCF and GDC has been reported that the best performance is from the composition of 50% and 60% LSCF [1,12,18]. The polarization reduces with the increasing GDC content to 50-60% and increases with higher GDC content over 60%. The cathode polarization depends on the composition as well as the morphologies. The GDC with the surface area of 5 m^2g^{-1} here shows the similar effects with previous reported works [1,13,19]. The fuel cell performance of 5LSCF-5GDC is higher than that of 6LSCF-4GDC and 4LSCF-6GDC. The 50% of GDC contents shows the highest fuel cell performance. The 5LSCF-5GDC shows the lowest polarization resistance of the composite electrode decreases by extending the TPB and increasing the oxygen diffusion. Furthermore, the

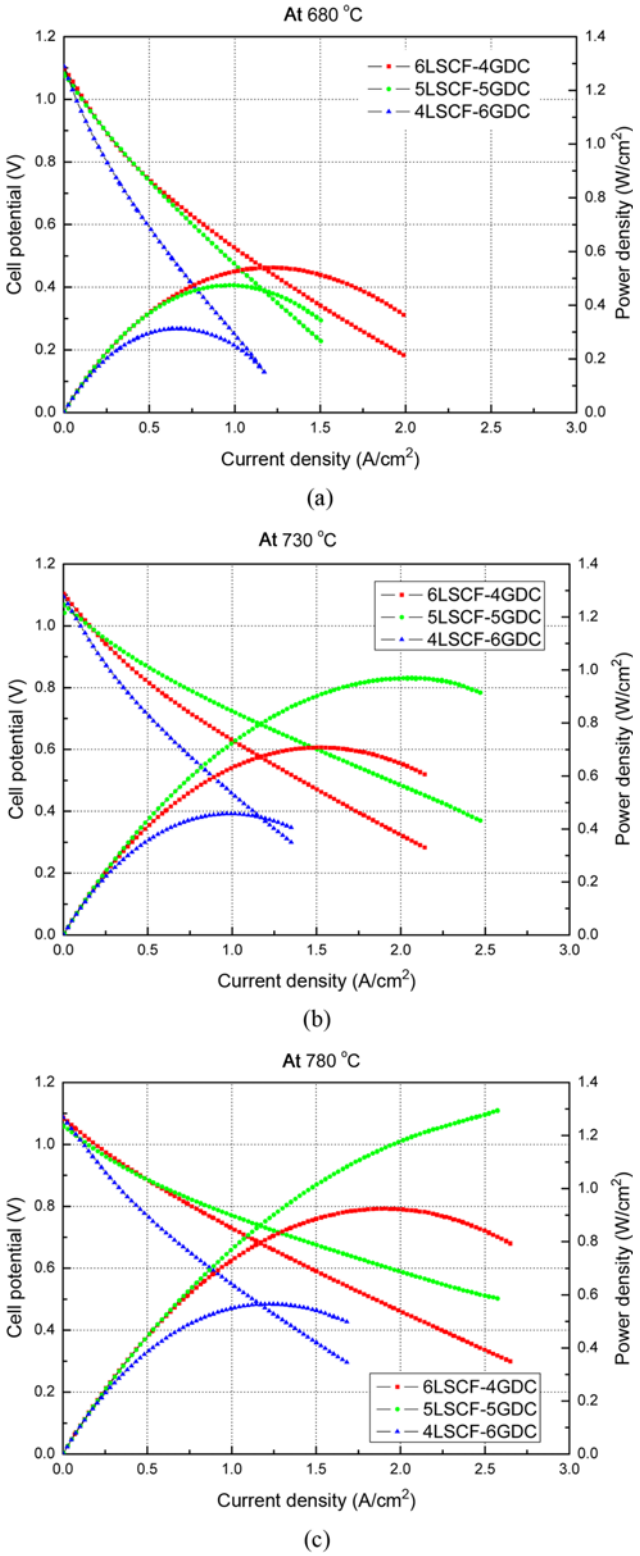

Fig. 3. Fuel cell performances of SOFCs with composite cathodes of (a) at 680 °C, (b) 730 °C, and (c) 780 °C.

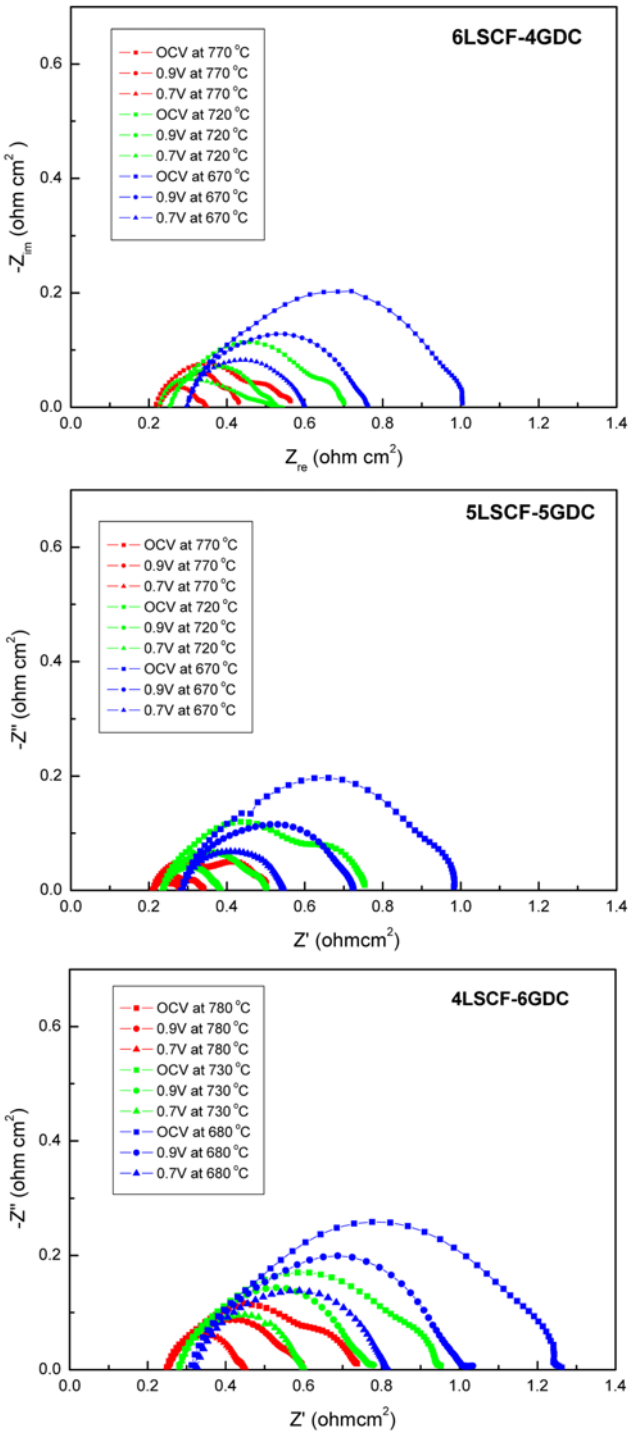

Fig. 4. Impedance measurements of the composite cathodes at 780 °C and open circuit voltage.

macro-pores introduced in the 5LSCF-5GDC composite cathode facilitate faster gas transport than 6LSCF-4GDC and 4LSCF-6GDC and accelerate electrode kinetics over 730 °C. At 680 °C, the fuel cell performance of 6LSCF-4GDC is almost same at a low current range and higher at a high current range than that of 5LSCF-5GDC.

To compare the polarizations of cells, the area-specific resistances (ASRs) of each cell are calculated from the linear portion of the current-voltage characteristics as they corresponded to the cell voltage from 1.0 V to 0.7 V [20]. The total values of the cells' ASRs comprise the ohmic resistance from the electrolyte, the electrodes, and the corresponding interfaces, as well as the polarization resistances at the electrodes. At 780 °C, the ASRs for cells with 6LSCF-4GDC, 5LSCF-5GDC, and 4LSCF-6GDC are 0.33 Ωcm^2, 0.24 Ωcm^2, and 0.57 Ωcm^2, respectively. The ASRs increase as the temperature decreases, such that at 680 °C, the ASRs of 6LSCF-4GDC, 5LSCF-5GDC, and 4LSCF-6GDC are 0.63 Ωcm^2, 0.64 Ωcm^2, and 1.04 Ωcm^2, respectively. At 680 °C, the ASRs of 6LSCF-4GDC and 5LSCF-5GDC are nearly identical. At that temperature, an electron conducting path may be effectively built by increasing the composition of LSCF.

The impedance values of composite cathodes were measured under open circuit voltage, 0.9 V and 0.7 V with an electrochemical impedance system. Fig. 4 shows the impedance spectra with different voltages and temperatures. The impedance spectra are obtained in the frequency range of 100 kHz to 0.1 Hz with applied AC voltage and amplitude of 100 mV at each temperature and cell potential of OCV, 0.9 V, and 0.7 V. The obtained impedances are fitted with the equivalent circuit in Fig. 5. The fitted results of the composite cathodes at OCV are presented in Fig. 6-8. R0 is from the ohmic resistance of the electrolyte, electrodes, and the connection wires; L is the inductance, which is attributed to the platinum current-voltage probes or the heating elements of the furnace used

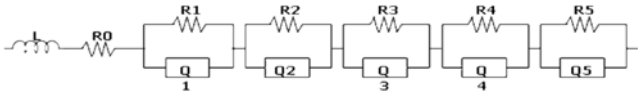

Fig. 5. Equivalent circuit for fitting model.

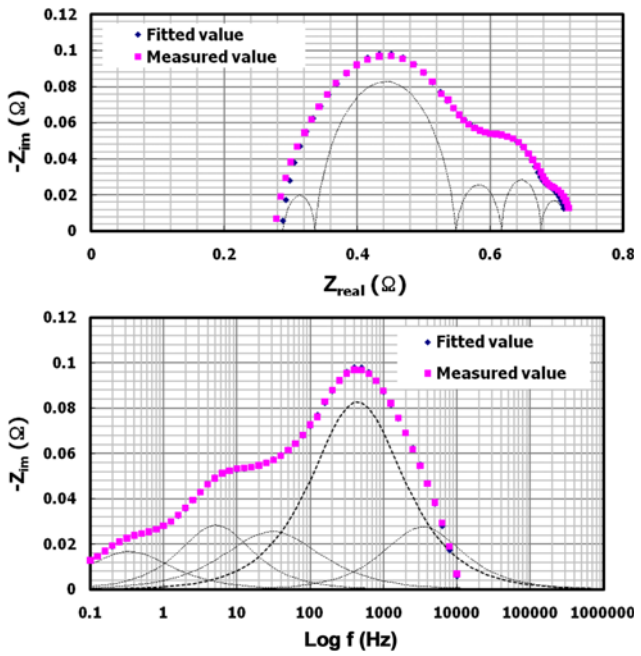

Fig. 6. Equivalent circuit and fitting results of the composite cathode at 780 °C and open circuit voltage, 6LSCF-4GDC composite cathode.

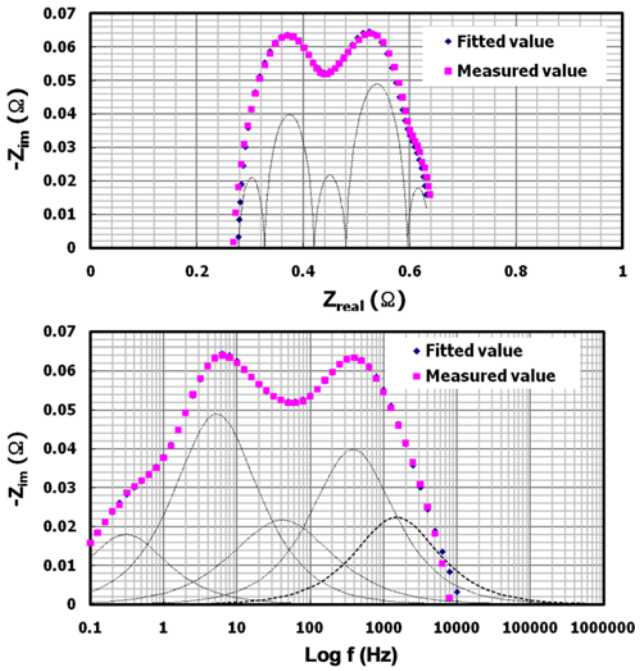

Fig. 7. Equivalent circuit and fitting results of the composite cathode at 780 °C and open circuit voltage, 5LSCF-5GDC composite cathode.

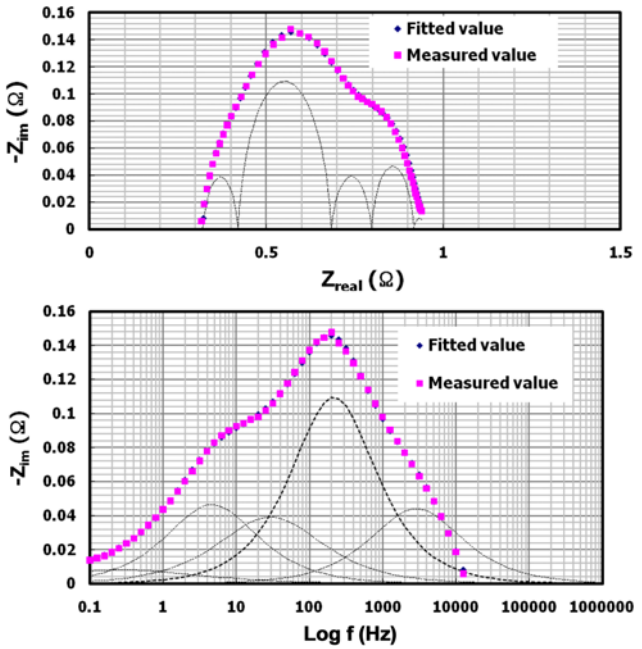

Fig. 8. Equivalent circuit and fitting results of the composite cathode at 780 °C and open circuit voltage, 4LSCF-6GDC composite cathode.

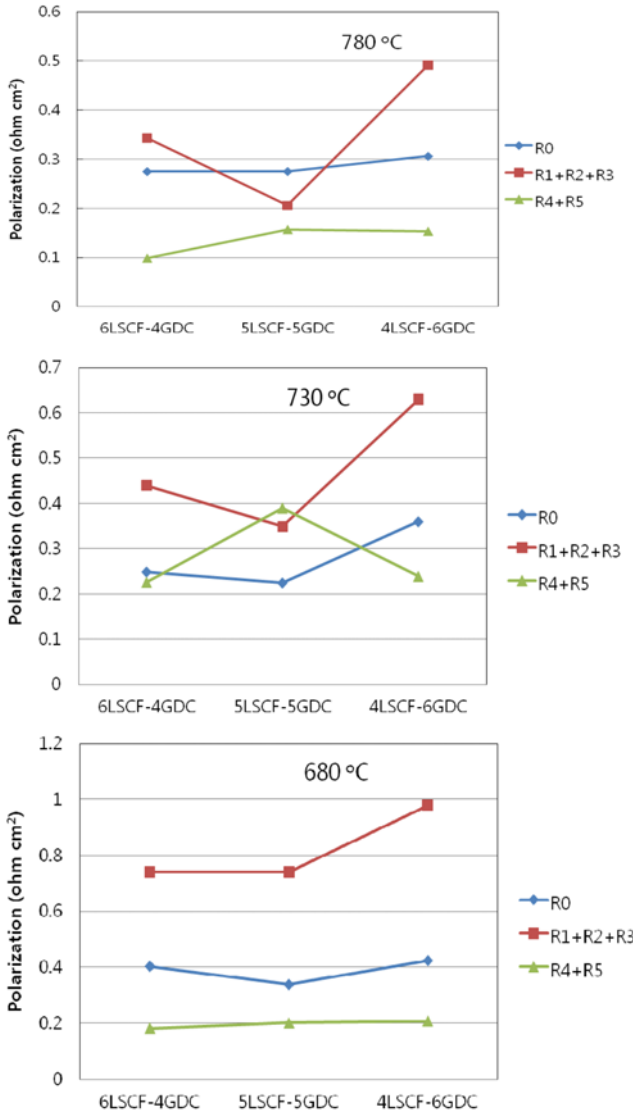

Fig. 9. Ohmic polarizations (R0), charge transfer polarizations (R1+R2+R3), and mass transfer polarizations (R4+R5) of composite cathodes as a function of temperature at open circuit voltage.

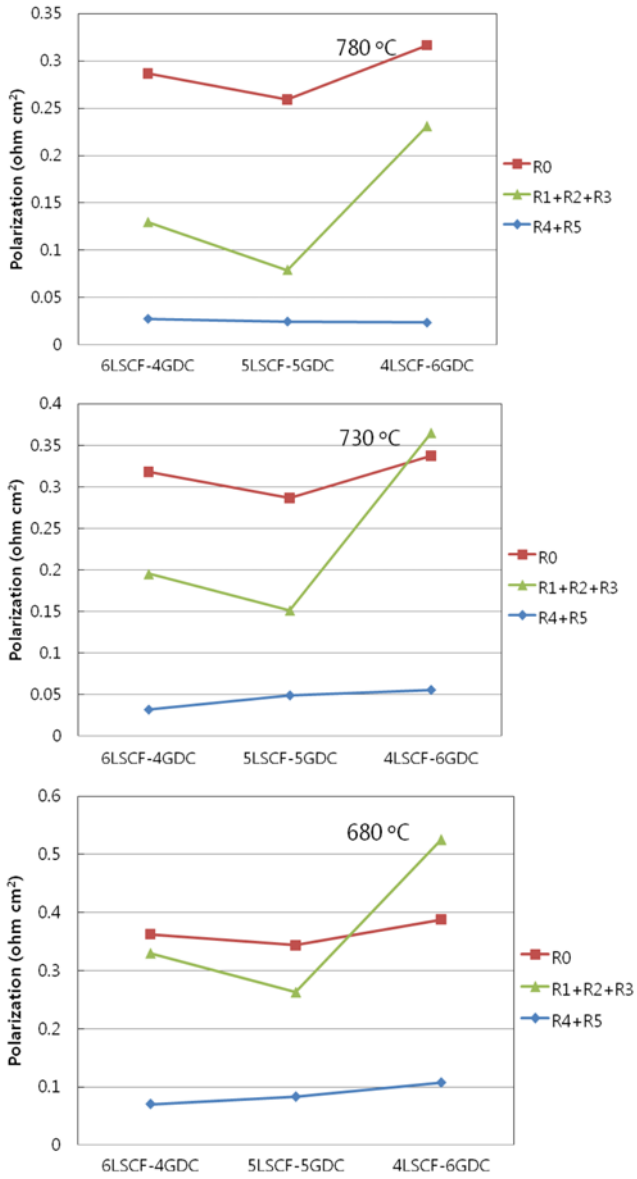

Fig. 10. Ohmic polarizations (R0), charge transfer polarizations (R1+R2+R3), and mass transfer polarizations (R4+R5) of composite cathodes as a function of temperature at 0.7 V.

to heat up the sample; (R1Q1) and (R3Q3) correspond to the gas diffusion coupled with the charge transfer reaction and ionic transport; (R2Q2) corresponds to the oxygen surface exchange kinetics and oxygen ion diffusivity at cathode; and (R4Q4) and (R5Q5) correspond to the gas diffusion reaction [21-23]. From Fig. 9, the ohmic resistances, (R0), of SOFCs with 6LSCF-4GDC, 5LSCF-5GDC, and 4LSCF-6GDC are similar at 780 °C. The ohmic resistance at 680 °C, the SOFC with 6LSCF-4GDC and 4LSCF-6GDC shows similar values. The ohmic resistances of composite cathodes may be compromised with ionic conductivity and electronic conductivity in terms of compositions. The charge transfer resistance, the sum of R1, R2 and R3, of the SOFC with 4LSCF-6GDC is the highest in all temperature. The charge transfer resistance, of 5LSCF-5GDC is lower than that of 6LSCF-4GDC at 780 °C and 730 °C. However, the charge transfer resistance of 5LSCF-5GDC shows a similar value with 6LSCF-4GDC at 680 °C. The mass transfer polarization, the sum of R4 and R5, of 5LSCF-5GDC shows a higher value than that of 6LSCF-4GDC. The fitted results at 0.7 V, as shown in Fig. 10, show the similar phenomena, which the 6LSCF-4GDC composite cathode has the higher charge transfer polarization and lower mass transfer polarization than the 5LSCF-5GDC. These phenomena can also be explained via the ambipolar conductivity model of porous composite cathodes, as developed by Dusastre et al. [1]. The optimum composition of LSCF and GDC for building ionic and electronic paths may be considered with particle size and composition [13]. The high electro-catalytic activity of LSCF and the formation of triple phase boundaries by adding 50 wt% of GDC shows the lowered charge transfer polarization and increased mass transfer polarization, when compared with the 6LSCF-4GDC, which results in the higher fuel cell performances. However, with decreasing temperature, the effects of charge transfer polarization are be-

coming more dominant and the 6LSCF-4GDC shows the similar fuel cell performance with the 5LSCF-5GDC. It is observed that the overall performance of a porous electrode is not only determined by the mixed conducting transport properties in the solid phase of the electrode, but also by the inherent catalytic property of the triple phase boundary, and by the gas transport to, or away, from the triple phase boundary [1]. To obtain optimized morphologies of porous composite cathodes, the composition and morphologies of the cathodes materials should be studied with consideration of the operating temperatures. In this study, the composite cathode with LSCF (surface area of 55 m^2g^{-1}) and GDC (surface area of 5 m^2g^{-1}) which shows the highest fuel cell performance at 780 °C and 730 °C is 5LSCF-5GDC, while 6LSCF-4GDC exhibits the highest performance at 680 °C.

CONCLUSIONS

$La_{0.6}Sr_{0.4}Co_{0.2}Fe_{0.8}O_{3-\delta}$-based porous composite cathodes with surface areas of 55 m^2g^{-1} were fabricated with GDC materials with a surface area of 5 m^2g^{-1}, as a function of GDC compositions. At 780 °C, the composite cathode formulated with 50 : 50 wt% LSCF and GDC showed the highest maximum power density of 1.29 Wcm^{-2}. At 680 °C, the cathode with 60 : 40 wt% LSCF and GDC showed the highest maximum power density of 0.92 Wcm^{-2}. For operating temperatures lower than 700 °C, porous composites containing a greater amount of LSCF materials are more effective. At such temperatures, GDC materials may be obstacles to building electron-conducting paths, which can also lead to an increase in the polarization. To obtain the highest fuel cell performance, the compositions of GDC materials for porous composite cathodes must be carefully selected in consideration of the operation temperature.

REFERENCES

1. V. Dusastre and J. A. Kilner, *Solid State Ionics*, **126**, 163 (1999).
2. D. Kus¡s¡cer, J. Holc, S. Hrovat and D. Kolar, *J. Eur. Ceram. Soc.*, **21**, 1817 (2001).
3. A. Mai, V. A. C. Haanappel, S. Uhlenbruck, F. Tietz and D. Stöver, *Solid State Ionics*, **176**, 1341 (2005).
4. A. Mai, V. A. C. Haanappel, S. Uhlenbruck, F. Tietz and D. Stöver, *Solid State Ionics*, **177**, 2103 (2006).
5. Y. Teraoka, H. M. Zhang, K. Okamoto and N. Yamazoe, *Mater. Res. Bull.*, **23**, 51 (1988).
6. J. Fleig, *J. Power Sources*, **105**, 228 (2002).
7. J. W. Hwang, J. Y. Lee, D. H. Jo, H. W. Jung and S. H. Kim, *Korean J. Chem. Eng.*, **28**, 143 (2011).
8. V. A. C. Haanappel, J. Mertens, D. Rutenbeck, C. Tropartz, W. Herzhof, D. Sebold and F. Tietz, *J. Power Sources*, **141**, 216 (2005).
9. S. B. Adler, J. A. Lane and B. C. H. Steele, *J. Electrochem. Soc.*, **143**, 3554 (1996).
10. J. A. Kilner, R. A. De Souza and I. C. Fullarton, *Solid State Ionics*, **86-88**, 703 (1996).
11. J. Fleig, *Annu. Rev. Mater. Res.*, **33,** 361 (2003).
12. V. V. Srdic, R. P. Omorjan and J. Seidel, *Mater. Sci. Eng. B.*, **116**, 119 (2005).
13. E. P. Murray, M. J. Sever and S. A. Barnett, *Solid State Ionics*, **148**, 27 (2002).
14. N. Gunasekaran, S. Saddawi and J. J. Carberry, *J. Catal.*, **159**, 107 (1996).
15. Y. Liu, H. Zheng, J. R. Liu and T. Zhang, *Chem. Eng. J.*, **89**, 213 (2002).
16. A. Dutta, J. Mukhopadhyay and R. N. Basu, *J. Eur. Ceram. Soc.*, **29**, 2003 (2009).
17. S. Shukla, S. Seal, R. Vij and S. Bandyopadhyay, *Nano Lett.*, **3**, 397 (2003).
18. J. H. Kim, Y. M. Park and H. Kim, *J. Power Sources*, **196**, 3544 (2011).
19. Y. Leng, S. Chan and Q. Liu, *Int. J. Hydrog. Energy*, **33**, 3808 (2008).
20. J. W. Kim, A. V. Virkar, K. Z. Fung, K. Mehta and S. C. Singhal, *J. Electrochem. Soc.*, **146**(1), 69 (1999).
21. H. Schichlein, A. C. Muller, M. Voigts, A. Krugel and E. Ivers-tiffee, *J. Appl. Electrochem.*, **32**, 875 (2002).
22. A. Leonide, V. Sonn, A. Weber and E Ivers-Tiffée, *J. Electrochem. Soc.*, **155**, B36 (2008).
23. Y. M. Park, J. H. Kim and H. Kim, *Int. J. Hydrog. Energy*, **36**, 5617 (2011).